Solvent Dynamics and Mechanism of Proton Transfer in Human Carbonic Anhydrase II

Samuel Toba,[†] Giorgio Colombo,[‡] and Kenneth M. Merz, Jr.*[,†]

Contribution from 152 Davey Laboratory, Department of Chemistry, The Pennsylvania State University, University Park, Pennsylvania 16802, and the Istituto di Biocatalisi e Riconoscimento Molecolare, CNR, via Mario Bianca 9, 20131, Milano, Italy

Received October 12, 1998

Abstract: In this paper we describe the first all-atom aqueous-phase MD simulations of human carbonic anhydrase II in three protonation states relevant to the rate-limiting intramolecular proton-transfer step. In particular, we have examined the zinc−water form of the enzyme (CHOH), the zinc−hydroxide form of the enzyme with a doubly protonated His-64 (COHH, the putative intramolecular proton-transfer proton-accepting residue), and the native zinc−hydroxide form (COH) of the enzyme (i.e., with an unprotonated His-64). From these MD simulations (up to ∼1 ns in length) we have studied in detail the dynamics of these three systems. Overall the dynamics of the three systems do not vary significantly (e.g., the active site region is rigid, the number of long-lived hydrogen bonds is constant, etc.) with the exception of COHH. In this case the residues that line the entrance to the active site cavity (near the location of His-64) undergo significantly higher fluctuations than in the CHOH and COH cases. It is postulated that this facilitates solvent and buffer exchange around His-64, thereby facilitating the intermolecular proton-transfer step. We also find that the motion of His-64 is limited in all three cases to occupying the "in" orientation (∼7 Å from the zinc ion, while the so-called "out" conformer is further away), which suggests that fluctuations of this residue between the in and out conformers have a limited influence on the intramolecular proton transfer. However, due to the limited time scales of our simulations, this needs to be examined in more detail. Importantly, though, we find that His-64 acts as a "gate-keeper" between the inner active site region (characterized by localized water molecules) and the outer (bulk) region, which is characterized by relatively freely diffusing water molecules. This function of His-64 has not been realized previously. In the inner active site we have identified relatively long-lived water bridges between the zinc-bound water or hydroxide and the imidazole or imidazolium side chain of His-64. The lengths of these bridges vary between two and six water molecules, and the preferred bridge depends on the protonation of the active site. We estimate that the probability of water bridge formation is low (at most ∼1.5 kcal/mol) and that water bridge formation is not the rate-limiting step in the proton-transfer process (transfer from zinc-bound water to an active site water is rate-limiting).

Introduction

Human carbonic anhydrase II (HCAII), which is present in the nonpigmented epithelial cells of the eye and red blood cells,[1] catalyzes the interconversion of carbon dioxide and bicarbonate plus a proton.[2] HCAII consists of a single polypeptide chain of 260 residues with a molecular weight of about 30 000. The active site is about 15 Å across and 15 Å deep with a catalytic zinc ion positioned at the bottom of the pocket.[3,4] HCAII is the most efficient ($k_{cat} = 10^{-6}$ s^{-1}) of the seven known isozymes of carbonic anhydrase found in higher vertebrates.[5] A thorough understanding of the catalytic mechanism of this "perfectly evolved enzyme" (based on k_{cat}/K_M) will and has provided important insights into catalysis.[6]

The chemistry of HCAII catalysis occurs in two distinct steps (ping-pong kinetics): (1) the nucleophilic attack of zinc-bound hydroxide at the carbonyl carbon of CO_2, generating bicarbonate ion, and (2) the regeneration of the zinc−hydroxide form of the enzyme from the zinc−water form following bicarbonate release (Figure 1).[1,7−9] The zinc ion is essential for catalytic activity and is tetrahedrally coordinated to three histidines (His-96, -94, and -119) and a hydroxide ion or water depending on

[†] The Pennsylvania State University.

[‡] Istituto di Biocatalisi e Riconoscimento Molecolare.

(1) Silverman, D. N.; Lindskog, S. The Catalytic Mechanism of Carbonic Anhydrase: Implications of a Rate-Limiting Protolysis of Water. *Acc. Chem. Res.* **1988**, *21*, 30−36.

(2) Kannan, K. K.; Petef, M.; Fridborg, K.; Cid-Dresdner, H.; Lövgren, S. Structure and Function of Carbonic Anhydrases. Imidazole Binding to Human Carbonic Anhydrase B and the Mechanism of Action of carbonic Anhydrases. *FEBS Lett.* **1977**, *73*, 115−119.

(3) Eriksson, A. E.; Jones, A. T.; Liljas, A. Refined Structure of Human Carbonic Anhydrase II at 2.0 Å Resolution. *Proteins* **1988**, *4*, 274−282.

(4) Håkansson, K.; Carlsson, M.; Svensson, L. A.; Liljas, A. The Structure of Native and Apo Carbonic Anhydrase II, and some of its Anion Ligand Complexes. *J. Mol. Biol.* **1992**, *227*, 1192−1204.

(5) Tashian, R. E. The Carbonic Anhydrases: Widening Perspectives on Their Evolution, Expression and Function. *BioEssays* **1989**, *10*, 186−192.

(6) Fersht, A. R. *Enzyme Structure and Mechanism*; W. H. Freeman and Co.: New York, 1985.

(7) Lindskog, S. In *Carbonic Anhydrase*; Lindskog, S., Ed.; Wiley: New York, 1983; pp 77−121.

(8) Lindskog, S.; Coleman, J. E. The Catalytic Mechanism of Carbonic Anhydrase. *Proc. Natl. Acad. Sci. U.S.A.* **1973**, *70*, 2505−2508.

(9) Christianson, D. W. Structural Biology of Zinc. *Adv. Protein Chem.* **1991**, *42*, 281−355.

10.1021/ja983579y CCC: $18.00
Published on Web 02/24/1999

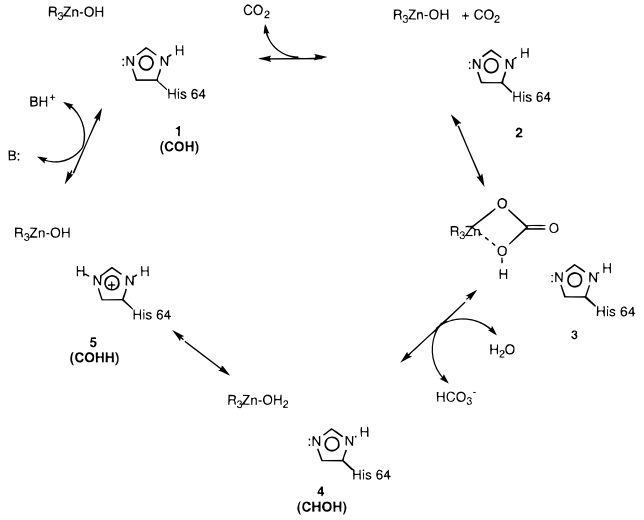

Figure 1. Proposed catalytic mechanism of HCAII.[7] The three simulation systems are labeled COH, COHH, and CHOH. In labeling the systems, the letter C stands for carbonic anhydrase followed by either *OH* for zinc-bound hydroxide (in C*OH* and C*OH*H) or *HOH* for zinc-bound water (in C*HOH*). The extra letter *H* in zinc-bound hydroxide (COH*H*) represents the protonated His-64.

the pH. The zinc−water form of the enzyme (with a pK_a value around 7) is within hydrogen-bonding distance of the OG of Thr-199, which is itself hydrogen bonded to Glu-106.[10] The rigidity of this hydrogen-bonding pattern appears to be important for rapid enzymatic catalysis[11] and inhibitor binding.[12−14]

The proton-transfer step in the catalytic cycle of CA remains the subject of ongoing debate in both the experimental and theoretical communities.[1,15] The most widely accepted mechanistic proposal involves His-64 which is located about 7.5 Å away from the zinc ion[3] in a hydrophilic region of the active site. His-64 is thought to be important for shuttling protons out of the active site, which requires that an intramolecular proton transfer between zinc-bound water and His-64 is required to generate the zinc−hydroxide form of the enzyme. This is followed by an intermolecular proton transfer with the aid of buffers in solution.[1,10,16,17] The mechanism proceeds by the transfer of one of the zinc−water protons to one of the water molecules present in the enzyme active site, thus generating the zinc−hydroxide form of the enzyme and a hydronium ion. This initial proton transfer sets off a chain of proton transfers (Figure 2) and results in eventual transfer of a proton to His-64. The proton transfer is the rate-limiting step at high buffer concentrations.[18] At low buffer concentrations, the proton release

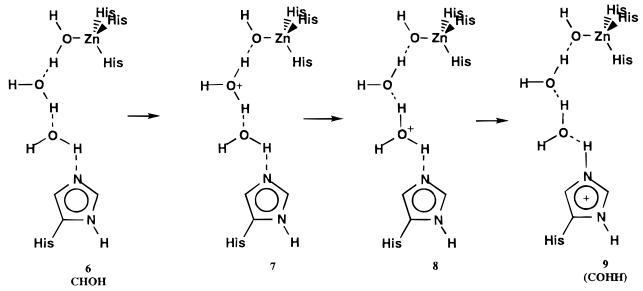

Figure 2. Proposed proton-transfer relay involving His-64.

into the medium is rate-limiting.[19] This mechanistic proposal is supported by both kinetic data[1] and experimental observation of several water molecules positioned between zinc−water and His-64.[3,4] On the basis of the examination of the zinc−hydroxide crystal structure of HCAII,[4] the shortest pathway between the zinc and His-64 involves two water molecules, but three water molecules could also form a bridge between the zinc ion and His-64 for a proton shuttle.[20] This is considered to be the "in" position for the His-64 side chain.[3] When some inhibitors are bound to the zinc ion, the imidazole ring of His-64 is moved approximately 3 Å away from the active site ("away" position). Point mutations of His-64 with non-proton-transferring amino acid residues reduce the rate of catalysis by 20-fold but do not completely eliminate enzyme activity.[21,22] The small activity of the mutant protein shows that His-64 may not be the only proton-transfer pathway essential for catalytic activity. Another mechanistic proposal involves the hydrogen bond network among Zn−H_2O, Thr-199, and Glu-106 in removing the proton and generating the nucleophilic Zn−OH. Although this mechanism is supported by the observation that this hydrogen bond network is present in all known carbonic anhydrases,[1,23,24] it is unlikely because it requires the elevation of the pK_a of Glu-106 from ca. 4 to >7.[18]

We have carried out a series of classical MD simulations, on fully solvated HCAII, which are aimed at garnering a better understanding of the mechanism of proton transfer and of the solvent dynamics in the active site of the protein. The partial charges for the active site region were obtained using a quantum mechanical/molecular mechanical (QM/MM) approach.[25] Of particular interest are water molecules in the active site that form water-mediated hydrogen bonds, cross-linking the residues

(10) Steiner, H.; Jonsson, B. H.; Lindskog, S. The Catalytic Mechanism of Carbonic Anhydrase. *Eur. J. Biochem.* **1975**, 253−259.

(11) Merz, K. M., Jr. Insights into the Function of the Zinc hydroxide-Thr 199-Glu106 Hydrogen Bonding Network in Carbonic Anhydrase. *J. Mol. Biol.* **1990**, *214*, 799−802.

(12) Eriksson, A. E.; Kylsten, P. M.; Jones, A. T.; Liljas, A. Crystallographic Studies of Inhibitor Binding Sites in Human Carbonic Anhydrase II: A Pentacoordinated Binding of the SCN^- Ion to the Zinc at High pH. *Proteins* **1988**, *4*, 283−293.

(13) Lindahl, M.; Svensson, L. A.; Liljas, A. Metal Poison Inhibition of Carbonic Anhydrase. *Proteins* **1992**, *15*, 177−192.

(14) Xue, Y.; Liljas, A.; Jonsson, B.-H.; Lindskog, S. Structural Analysis of the Zinc Hydroxide-Thr-199-Glu-106 Hydrogen-Bond Network in Human Carbonic Anhydrase II. *Proteins* **1993**, *17*, 93−106.

(15) Kannan, K. K. In *Structure and Function of Carbonic Anhydrases*; Kannan, K. K., Ed.; Pergamon Press: Oxford, 1981; Vol. 1, pp 165−181.

(16) Jonsson, B.-H.; Steiner, H.; Lindskog, S. Participation of Buffer in the Catalytic Mechanism of Carbonic Anhydrase. *FEBS Lett.* **1976**, *64*, 310−314.

(17) Tu, C. K.; Wynns, G. C.; Silverman, D. N. *J. Biol. Chem.* **1989**, *264*, 12389−12393.

(18) Silverman, D.; Vincent, S. H. Proton Transfer in the Catalytic Mechanism of Carbonic Anhydrase. *CRC Crit. Rev. Biochem.* **1983**, *14*, 207−255.

(19) Lindskog, S.; Behravan, G.; Engstrant, C.; Forsman, C.; Jonsson, B.; Liang, Z.; Ren, X.; Xue, Y. In *Carbonic Anhydrase: From Biochemistry and Genetics to Physiology and Clinical Medicine*; Lindskog, S., Behravan, G., Engstrant, C., Forsman, C., Jonsson, B., Liang, Z., Ren, X., Xue, Y., Eds.; Weinheim, 1991; pp 1−13.

(20) Lesburg, C. A.; Christianson, D. W. *J. Am. Chem. Soc.* **1995**, *117*, 6838.

(21) Tu, C.; Silverman, D. N.; Forsman, C.; Jonsson, B.-H.; Lindskog, S. Role of Histidine 64 in the Catalytic Mechansim of Human Carbonic Anhydrase II Studied with a Site-Specific Mutant. *Biochemistry* **1989**, *28*, 7913−7918.

(22) Forsman, C.; Behravan, G.; Jonsson, B.-H.; Liang, Z.; Lindskog, S.; Ren, X.; Sandström, J.; Wallgren, K. Histidine 64 is not Required for High CO_2 Hydration Activity of Human Carbonic Anhydrase II. *FEBS Lett.* **1988**, *229*, 360−362.

(23)) Åqvist, J.; Warshel, A. Computer Simulation of the Initial Proton-Transfer Step in Human Carbonic Anhydrase I. *J. Mol. Biol.* **1992**, *224*, 7−14.

(24) Pocker, Y.; Sarkanen, S. Carbonic Anhydrase: Structure, Catalytic Versatility, and Inhibition. *Adv. Enzymol.* **1978**, *47*, 149−274.

(25) Hartsough, D. S.; Merz, K. M., Jr. Dynamic Force Field Models: Molecular Dynamics Simulations of Human Carbonic Anhydrase II Using a Quantum Mechanical/Molecular Mechanical Coupled Potential. *J. Phys. Chem.* **1995**, *99*, 11266−11275.

involved in the proton transfer. Specifically, we have studied the three intermediate stages of proton transfer in HCAII in the absence of substrate. The three systems are depicted as stages **4**, **5**, and **1** in Figure 1. We employed the "bonded" approach which involves placing explicit bonds between the zinc ion and its surrounding ligands.[26] The model has been shown to be successful in maintaining the correct coordination for the metal ion as well as giving an accurate model of the electrostatic interactions within HCAII. This approach allows us to explore the structural and dynamic characteristics of the intermediate stages in detail.

In this paper, we address a number of important issues involving the proton-transfer mechanism in HCAII. We report our findings on the network of water molecules around the zinc ion, the conformation of His-64 upon the change in protonation state of the zinc-bound water and His-64, and the average lifetime of water bridge formation between zinc-bound water/hydroxide and His-64. The solvent effects on the structure and dynamics of the protein residues will also be addressed.

Computational Methods

We have set up three systems representing the different intermediates in the catalytic pathway. The first is the zinc−water form with a singly protonated His-64 (CHOH, **4** in Figure 2), the second is the zinc−hydroxide form with a doubly protonated His-64 (COHH, **5** in Figure 2), and the third is the zinc−hydroxide form with a singly protonated His-64 (COH, **1** in Figure 2). In labeling the systems, the letter C stands for carbonic anhydrase followed by either *OH* for zinc-bound hydroxide (in C*OH* and C*OH*H) or *HOH* for zinc-bound water (in C*HOH*). The extra letter *H* in the zinc-bound hydroxide system (COH*H*) represents the doubly protonated His-64. Starting coordinates were obtained from the high-resolution (1.54 Å) experimental crystal structure of Håkansson et al. (Protein Data Bank reference 2CBA).[4] The "in" conformation of His-64 (solvent-exposed ND1 atom) in the crystal structure shows a clear water bridge network to the zinc ion, and hence, this conformation was selected as the starting point for our simulations. We have used the same X-ray structure for both the zinc−water and the zinc−hydroxide simulations for the purpose of consistency. In addition, it has been found that the three-dimensional structure of HCAII is generally similar at different pH values.[27]

Partial Charges. Partial charges for the three histidines and the zinc ion were calculated using the QM/MM coupled potential method[28−30] followed by electrostatic potential fitting (ESP).[31] These calculations were carried out using ROAR 1.0.[32] We have used standard AMBER[33] all-atom force field parameters for the MM region. Similar to the work of others, we have used link atoms to cap exposed valence sites due to bonds which cross the QM−MM boundary.[29,34] In this method the QM region of the system is treated as a closed shell molecule with no exposed valence sites. In our system the imidazole ring is capped by a hydrogen atom at the CB carbon atom. These carbon atoms (three total) are then bonded to their respective CA carbon atoms through molecular mechanical bonds (using a standard AMBER carbon−carbon parameter set) between the two carbon atoms. When a residue was split between the QM and MM regions, the partial charges of that residue were modified to maintain the charge neutrality of the MM region.[25] The net charge of the QM region is set to +1 for the zinc−hydroxide systems (Zn = +2, zinc−hydroxide = −1, histidines = 0) and +2 for the zinc−water system (Zn = +2, zinc−water = 0, histidines = 0) during the QM/MM energy minimization. The nonbonded interactions between the capping atoms and the remainder of the protein molecule are not evaluated.

Table 1. Summary of the Setup of the Starting Configurations

molecule type	COH	COHH	CHOH
X-ray water	220	220	220
added water	10 103	10 103	10 103
zinc charge	0.803	0.803	0.890
added chloride ions		1	1

TIP3P water molecules were added, where possible, around the active site zinc atom to a distance of 22 Å using the EDIT module of AMBER 4.0.[35] Minimization of all atoms within 15 Å of the zinc ion (200 steps of steepest descent and 800 steps of conjugate gradient) for all three systems were carried out using the QM/MM method. During the minimization, the active site residues His-94, -96, and -119 and the active site zinc atoms and its fourth ligand (hydroxyl or a water molecule) were treated as QM atoms using the PM3 Hamiltonian. This approach has the advantage in that it includes environmental polarization effects (i.e., explicit inclusion of the enzyme and the solvent environments). The PM3 semiempirical Hamiltonian has been shown to be an effective method in our previous QM/MM studies[25,36] and, hence, our choice of the coupled PM3/MM method in the present context. Following energy minimization, the QM atomic charges were calculated using MNDO ESP calculations.[37] While PM3 has been found to be superior in reproducing the structure, MNDO has been found to be more accurate in reproducing charges.[26] The charges obtained for the capping atoms were divided and spread out in their respective histidine residues. This "bonded" approach of incorporating zinc and its ligands' charges has been shown to be capable of reproducing the active site geometry in HCAII while the approach in which formal charges were used resulted in five- or six-coordinate zinc.[26] The partial charges calculated for the zinc−hydroxide active site in the COH system were also used for the zinc−hydroxide region in the COHH systems. The partial charges for the CHOH system were obtained from ESP-calculated charges determined at the 300 ps instantaneous trajectory structure of COH after replacement of hydroxide by water in the QM region (see below for more details).

MD Setup. The protein and water molecules of the crystal structures were solvated in a TIP3P water box to generate the COH system. Any water molecules that came within 3.0 Å of a protein atom were removed. This resulted in the protein being solvated by 220 X-ray water molecules and 10 103 additional water molecules (Table 1). The AMBER[33] all atom representation was used for the protein, except for the active site region, where we have used the bond and angle parameters of Hoops et al.[26] in the COH and COHH systems. An

(26) Hoops, S. C.; Anderson, K. W.; Merz, K. M. J. Force Field Design of Metalloproteins. *J. Am. Chem. Soc.* **1991**, *113*, 8262−8270.

(27) Nair, S. K.; Calderone, T. L.; Christianson, D. W.; Fierke, C. A. Altering the Mouth of a Hydrophobic Pocket. Structure and Kinetics of Human Carbonic Anhydrase II Mutants at Residue Val-121. *J. Biol. Chem.* **1991**, *266*, 17320−17325.

(28) Stanton, R. V.; Hartsough, D. S.; Merz, K. M., Jr. An Examination of a Density Functional/Molecular Mechanical Coupled Potential. *J. Comput. Chem.* **1994**, *16*, 113−128.

(29) Field, M. J.; Bash, P. A.; Karplus, M. A Combined Quantum Mechanical and Molecular Mechanical Potential for Molecular Dynamics Simulations. *J. Comput. Chem.* **1990**, *11*, 700−733.

(30) Thompson, M. A. A QM/MM Molecular Dynamics Study of the Potential of Mean Force for the Association of K^+ with Dimethyl Ether in Aqueous Solution. *J. Am. Chem. Soc.* **1995**, *117*, 11341−11344.

(31) Besler, B. H.; Merz, K. M. J.; Kollman, P. A. Atomic Charges Derived from Semiempirical Methods. *J. Comput. Chem.* **1990**, *11*, 431−439.

(32) Cheng, A.; Stanton, R. S.; Vincent, J. J.; Damodaran, K. V.; Dixon, S. L.; Hartsough, D. S.; Best, S. A.; Merz, K. M. J. ROAR 1.0, 1997.

(33) Cornell, W. D.; Cieplak, P.; Bayly, C. I.; Gould, I. R.; Merz, K. M., Jr.; Ferguson, D. M.; Spellmeyer, D. C.; Fox, T.; Caldwell, J. W.; Kollman, P. A. A Second Generation Force Field for the Simulation of proteins, Nucleic Acids, and Organic Molecules. *J. Am. Chem. Soc.* **1995**, *117*, 5179−5197.

(34) Singh, U. C.; Kollman, P. A. A Combined *Ab initio* Quantum Mechanical and Molecular Mechanical Method for Carrying out Simulations on Complex Molecular Systems: Applications to the $CH_3Cl + Cl^-$ Exchange Reaction and Gas-Phase Protonation of Polyethers. *J. Comput. Chem.* **1986**, *7*, 718−730.

(35) Pearlman, D. A.; Case, D. A.; Caldwell, J. C.; Seibel, G. L.; Singh, U. C.; Weiner, P.; Kollman, P. A. AMBER 4.0, University of California, San Francisco, 1991.

(36) Merz, K. M., Jr.; Banci, L. Binding of Bicarbonate to Human Carbonic Anhydrase II: A Continuum of Binding States. *J. Am. Chem. Soc.* **1997**, *119*, 863−871.

(37) Merz, K. M., Jr.; Besler, B. H. MOPAC 5.0 ESP. *QCPE Bull.* **1990**, *10*, 15.

adjusted angle parameter (ND−Zn−OW) was found to be necessary to retain the experimentally observed tetrahedral zinc in CHOH (60 versus the 20 (kcal/mol)/Å^2 used for the COH and COHH systems) due to the higher charge on the zinc ion in the zinc−water (CHOH) system (+0.89 versus +0.80 for COH and CHOH). All the torsions associated with the zinc−ligand bonds were set to zero as in Hoops et al.[26] The calculated ESP charges for the active site residues were included in the representation of the protein/water system. The resulting system was minimized for 1000 steps prior to the MD simulations. The MD simulations were carried out using the ROAR 1.0[32] module from the AMBER[38] suite of programs. The temperature was raised from 0 to 300 K during the first 15 ps of simulation, and the temperature and pressure were then maintained at 300 K and 1 atm using the Nosé−Hoover chain algorithm for temperature and pressure coupling.[39] Ewald sums and long-range van der Waals corrections were used for the accurate treatment of long-range electrostatic and long-range van der Waals interactions, respectively. A K_{max} value of 8 was used along with a nonbond pairlist cutoff of 10 Å, and a 50-step nonbonded pairlist update was used. SHAKE[40] was used to constrain bond lengths at their equilibrium value, and a time step of 1.5 fs was employed. In all cases periodic boundary conditions were applied. The COH system was equilibrated for 750 ps, and the last 300 ps of the trajectory was saved for analysis.

On the basis of the convergence of the dimensions of the COH simulation box, we feel that the protein had sufficiently adjusted to its solvent environment at ∼300 ps. Hence, the 300 ps instantaneous structure of the COH system was used as the starting structure for both the COHH and CHOH systems. The singly protonated His-64 in the COH system was mutated into a doubly protonated His-64 in the COHH system. One chloride ion was added as a counterion to the COHH system to neutralize the charge. In the CHOH system, the zinc-bound hydroxide in the COH system was mutated into a zinc-bound water. All other water molecules from the COH system were retained and placed into the COHH and CHOH systems. The COHH and CHOH systems were then reminimized for another 1000 steps (200 steps of steepest descent and 800 steps of conjugate gradient) prior to obtaining the ESP charges for the active site residues. The MD simulation protocols for the COHH and CHOH systems were identical to that for the COH system. The equilibration period was 300 ps, and the last 300 ps of coordinates were saved for analysis every 50 time steps. The total MD simulation time was 1050 ps for COH, 600 ps for COHH, and 600 ps for CHOH.

Results and Discussion

Protein Root-Mean-Square Deviation and Flexibility. The RMS deviation (RMSD) is a measure of the deviation of the instantaneous protein structure from its crystal structure. We have calculated the RMSDs for the three systems, and they are shown in Figure 3. The COHH and CHOH systems appear to have reached equilibrium at ca. 300 ps, and the COH system is equilibrated at ca. 750 ps. Why the COH simulation required a longer simulation time scale to reach equilibrium with respect to RMS is not completely clear; however, both the COHH and CHOH systems were started from the 300 ps structure of COH. Thus, the protein and the solvent structure had already been "preequilibrated" for those two systems. It is also possible that part of the reason for a longer equilibration time in COH is due to the mobility of ∼10 water molecules within the active site. We observe that the solvent diffusion coefficient within the active site (<9 Å from the zinc ion) is much higher in COH than in COHH or CHOH (see Figure 12). Nevertheless, all three systems do not deviate significantly from the crystal structure and have average RMSD values typically seen in protein simulations.[25,41] The average RMSD values after equilibration for all protein atoms and backbone atoms are given in Table 2. The calculated radius of gyration values show no significant changes for the protein shape in all three systems relative to the X-ray structure (Table 2). This is to be expected given that

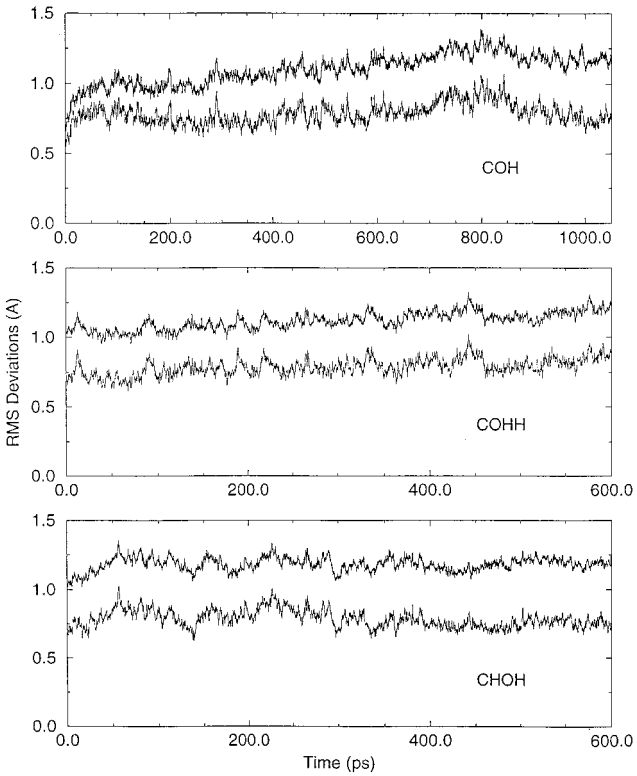

Figure 3. RMS deviations between the instantaneous computed structures and the crystal structure for all residues as a function of time. In all cases, the upper curve is for all atoms, while the lower curve is for backbone atoms only. The starting structure for COHH and CHOH was obtained from the 300 ps instantaneous structure of COH. For the average values of the RMS deviations, see Table 2.

Table 2. Summary of the RMS Deviations, Radius of Gyration Data, RMS Fluctuations, and Hydrogen-Bonding Data from the Simulations

	COH	COHH	CHOH
	RMSD (Å)		
total	1.20	1.16	1.18
backbone	0.82	0.81	0.75
	Rad_{gyr} (Å)		
protein average[a]	17.60	17.58	17.54
	RMSF (Å)		
total	1.69	2.21	1.81
backbone	1.58	2.11	1.70
His-64	1.55	2.24	1.62
His-94	1.38	1.64	1.21
His-96	1.39	1.42	1.47
His-119	1.28	1.23	1.19
Glu-106	1.31	1.11	1.58
Thr-199	1.34	1.13	1.50
upper hydrophobic core	1.52	1.85	2.03
lower hydrophobic core	1.70	2.55	1.47
	Hydrogen Bonding		
total	1174	1209	1195
≥90%	154	155	155

[a] The rad_{gyr} value of the protein from X-ray is 17.5 Å.

(38) AMBER 5.0, University of California, San Francisco, 1997.

(39) Cheng, A.; Merz, K. M., Jr. Application of the Nose-Hoover Chain Method to the Study of Protein Dynamics. *J. Phys. Chem.* **1996**, *100*, 1927−1937.

(40) van Gunsteren, W. F.; Berendsen, H. J. C. Algorithm for Macromolecular Dynamics and Constraint Dynamics. *Mol. Phys.* **1977**, *34*, 1311.

(41) van Gunsteren, W. F.; Berendsen, H. J. C. Computer Simulation as a Tool for Tracing the Conformational Differences between Proteins in Solution and in the Crystalline State. *J. Mol. Biol.* **1984**, *176*, 559−564.

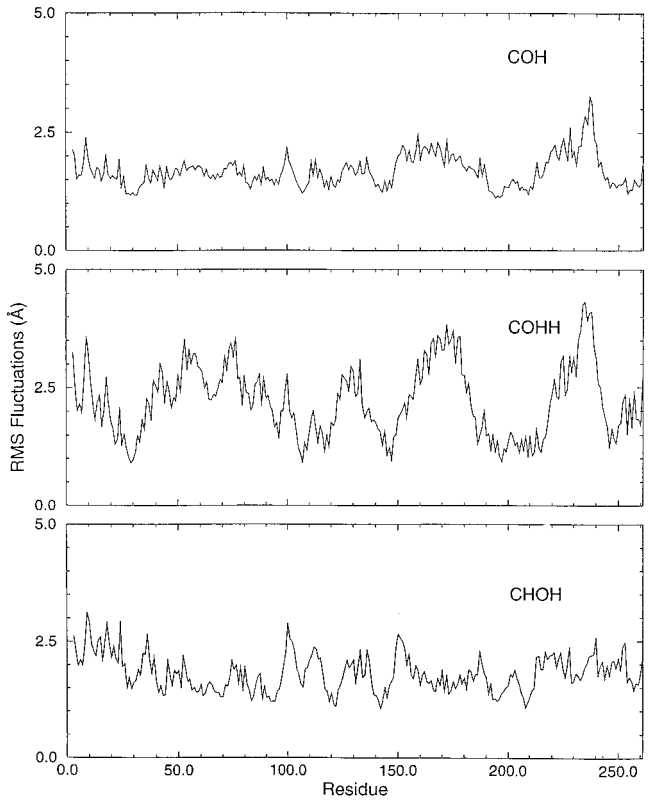

Figure 4. RMS fluctuations per residue from the time-averaged structure. Values averaged over the last 300 ps of each simulation relative to the averaged instantaneous structures.

the perturbation in the three systems is only minor. The protein remained globular, and no unwinding or denaturation was observed.

To obtain insights into the fluctuations of HCAII, we have also calculated the RMS flexibility (RMSF) of the protein by comparing the instantaneous protein structure to the average protein structure over the last 300 ps of the trajectory (Figure 4). The average RMSFs are given in Table 2. The RMSF for the backbone atoms does not differ significantly from the RMSF for the total atoms in the protein. This indicates that the protein fluctuations are not confined to the side chain motions alone, but rather, the protein backbone also undergoes significant fluctuations. In the three postulated stages of proton transfer in HCAII (see Figure 2), we can consider CHOH as one of the "native" states in the proton-transfer process, while COHH is an intermediate stage, which results in the native COH stage where the protein is ready to accept CO_2. The average flexibility of the protein is significantly higher in the COHH system when compared to the CHOH and COH systems. The higher flexibility in COHH is especially evident for the residues located at the surface of the protein (e.g., His-64; see below). It is possible that the increased flexibility in COHH may play a role in the intermolecular proton-transfer process. As the protein in COHH undergoes high fluctuations, it perturbs the solvent molecules surrounding the protein. This perturbation would in turn allow greater solvent or proton acceptor (e.g., buffers) exchange around the protein and, hence, potentially facilitate the intermolecular proton transfer.

Analyzing the RMSF of the active site reveals some interesting insights. Not surprisingly, the three histidyl ligands (His-94, -96, -119) remained fairly rigid in all three systems (Table 2). The rigidity of the histidyl residues shows the ability of the protein to retain the active site geometry necessary for CO_2 hydration (or bicarbonate dehydration) activity. However, His-64, located at the interface of the active site and bulk solvent region, shows greater fluctuations in COHH as opposed to COH and CHOH. The conformational flexibility of His-64 has been proposed as the primary factor that is important in the proton relay mechanism.[27,42] The higher flexibility of His-64 in COHH is not surprising given that the His-64 is doubly protonated and ready to transfer a proton to the bulk solvent. The greater flexibility of His-64 allows the imidazolium side chain to always reposition itself for optimum interactions between the active site solvent environment and the constantly moving water "environment" of the bulk solvent.

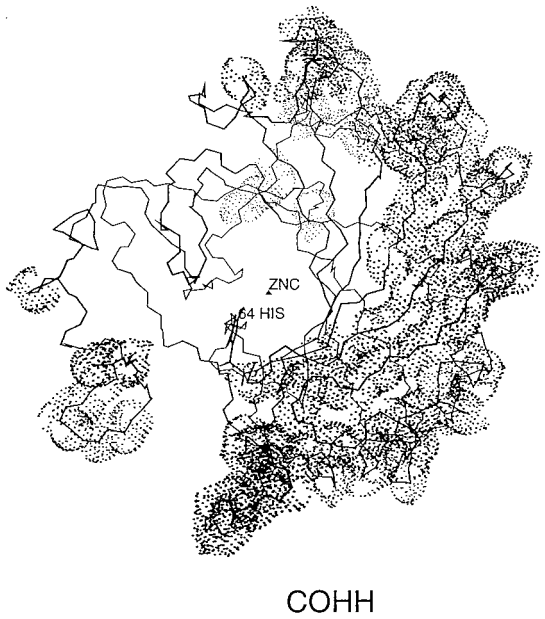

Figure 5. RMS flexibility of the protein in COHH. Only backbone atoms are shown for all residues except His-64 which is situated at the mouth of the active site cavity. The residues with high flexibility are shown with their van der Waals sphere, and the protein can be visualized as a "baseball in a pitcher's glove"; the baseball is the active site region with low flexibility, and the pitcher's glove is the region with high flexibility.

The RMSF per residue plot for COHH also shows very distinct regions of high and low flexibility. We divided the RMSF per residue of the protein in COHH into three separate regions: low (RMSF < 1.5 Å), intermediate (1.5 Å < RMSF < 2.5 Å), and high (RMSF > 2.5 Å). We observed an interesting correlation between the separate RMSF regions and distinct regions in the protein. We find that residues with low RMSF in COHH are confined to residues in the region surrounding the zinc ion. The zinc ion is located in a cavity buried in the protein that is partially accessible to the bulk solvent.[3] The residues with low flexibility form the conical-shaped cavity surrounding the zinc ion. It appears that the low flexibility of the residues surrounding the active site and the zinc ion helps to lock the active site residues into a favorable conformation for optimum catalytic activity. On the opposite end of the spectrum, the residues with high RMSF are also confined to a distinct region of the protein. This region is solvent exposed and located primarily in the "lower half" of the protein and extending on one side to the "upper half" of the protein (see Figure 5). The protein can be visualized as "a baseball in a pitcher's glove" where the low-flexibility active site cavity region is represented as the baseball and is surrounded, on one

(42) Fierke, C. A.; Calderone, T. L.; Krebs, J. F. Functional Consequences of Engineering the Hydrophobic Pocket of Carbonic Anhydrase II. *Biochemistry* **1991**, *30*, 11054−11063.

side, by the high-flexibility region represented as the pitcher's glove (Figure 5). We find that the increased flexibility of this region is possibly due to the high ratio of hydrophilic residues to hydrophobic residues (HL/HB). Our calculations show that while the low- and intermediate-RMSF regions only yield HL/HB ratios of 0.87 and 0.74, respectively, the high-RMSF region has an unusually high HL/HB ratio of 1.72. The third region containing residues with intermediate RMSF values is located between the residues with high and low RMSF values, and comprises both solvent-exposed and buried residues. The HL/HB ratio of this intermediate-RMSF region is similar to that of the low-RMSF region. Given the strategic placement of these intermediate-RMSF residues, it is possible that this intermediate-RMSF region functions as a buffer region to protect the active site region from the residues in the high-RMSF region and the surrounding bulk water. Thus, this buffering action of the residues in the intermediate-RMSF region might help preserve the structural integrity of the protein active site necessary for its catalytic activity. This further supports the notion that the role of the surface motion in COHH is to "stir" the surface water molecule near the mouth of the active site cavity and thus help facilitate intermolecular proton transfer, through water and buffer exchange, without affecting the active site residues.

On the other hand, the regions of high and low RMSF in COH or CHOH are not as distinct as in COHH. This is, again, due to the different roles adopted by the protein at the different stages of proton transfer. The high-flexibility motion of the surface residues is only critical in COHH and to a lesser extent in COH. Not surprisingly, the regions with high flexibility (residues 150−179 and 217−242) in COH are also surface-exposed residues. These residues are located on one side of the protein surface with His-64 located nearby at the "edge" of the region. It is possible that the flexibility of the residues in this region facilitates the diffusion of solvent, buffer, or substrate (CO_2) molecules into the active site cavity. No region with significant surface residue fluctuation was observed in CHOH. It is worth noting that the regions with relatively low flexibility are conserved in all three systems (residues 27−33, 105−109, 117−123, 140−145, and 191−197) and, not surprisingly, are located surrounding the active site residues.

It has also been observed that HCAII contains two "hydrophobic cores" and that each is located in the "upper" and "lower" halves of the protein.[3] The lower hydrophobic core is larger than the upper core and is situated just below the zinc-binding histidines in the active site (see the orientation in Figure 5). This lower cluster contains 34 residues and is mainly made up of the aromatic Phe residues (Phe-66, -70, -93, -95, -176, -179, and -226 and Trp-97); the smaller upper hydrophobic core near the N-terminal region encloses Tyr-7 and includes residues Trp-5, Trp-16, and Phe-20.[3] These residues are highly conserved in all available amino acid sequences of carbonic anhydrases.[43] In our simulations, the lower hydrophobic core remains buried and the upper hydrophobic core remains solvent exposed. The solvent-accessible surface area value (SASA) shows the buried and solvent-exposed nature of the lower and upper hydrophobic cores, respectively (Table 3). While one would expect that solvent-exposed residues would generally have the higher RMSF, we observe that the COHH system has an unusually high RMSF for the buried lower hydrophobic core. We attribute this to the presence of the protonated His-64 in the core of the protein. The residues of the lower hydrophobic core are in close proximity to the zinc−histidyl ligands as well as His-64.

(43) Hewett-Emmett, D.; Hopkins, P. J.; Tashian, R. E.; Czelusniak, J. Origins and Molecular Evolution of the Carbonic Anhydrase Isozymes. *Ann. N. Y. Acad. Sci.* **1984**, *429*, 61−75.

Table 3. Summary of the Distance of Zinc from Side Chain Nitrogens of His-64 and SASA

	X-ray	COH	COHH	CHOH
		Distance (Å)		
Zn−ND@64	7.4	7.9	7.9	7.6
Zn−NE@64	9.0	8.8	9.2	8.8
		SASA (Å^2)		
upper-SASA	131.4	144.5	142.8	152.9
lower-SASA	34.2	49.8	40.6	38.5
His-94	21.72	27.52	29.98	28.98
His-96	4.15	3.87	6.50	4.44
His-119	3.90	1.52	1.70	1.71

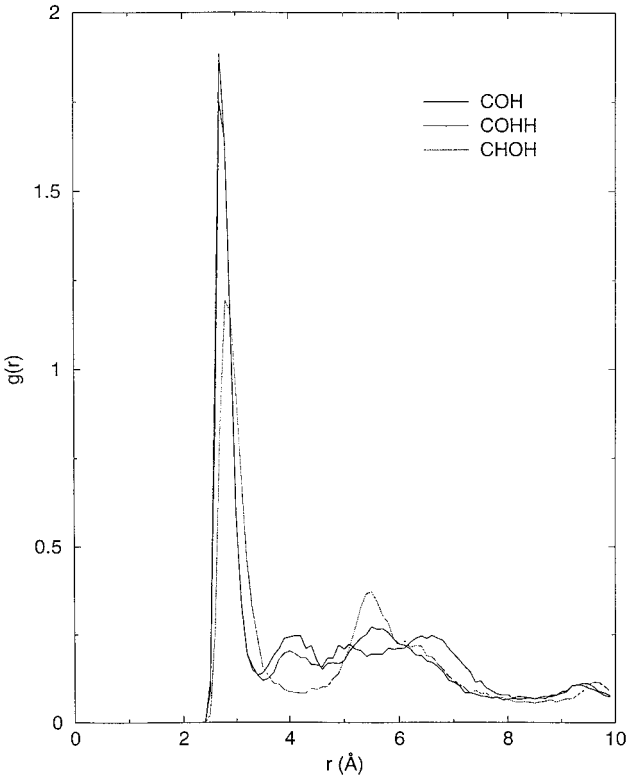

Figure 6. Pair distribution functions for the oxygen in zinc−water/hydroxide to the oxygens in the surrounding water molecules.

Potentially, the positively charged imidazolium of protonated His-64 generates strong electrostatic interactions with the nearby environment in the interior of the COHH system. This results in the lower hydrophobic core residues undergoing higher conformational fluctuations in response to the charged imidazolium ion. This charge perturbation is not observed in the COH and CHOH system where the His-64 is singly protonated. This "lack" of perturbation arising from charged residues reduces the conformational flexibility of the lower hydrophobic residues. These simulations have provided us with further insight into the effect that a charged environment might have on hydrophobic packing in a protein.

Solvation of Zinc Ion, Zinc−Water/Hydroxide, and Thr-199. Pair distribution functions (pdfs) allow us to obtain insights into the extent of water penetration and solvent ordering around the atoms of interest in the active site. Our pdfs between the oxygen of the zinc−water/hydroxyl group and the oxygen atom of the water molecules show three peaks for the COH system (Figure 6); the three solvation shells are located 2.7, 4.1, and 5.5 Å away from the oxygen of the zinc−hydroxide. In COHH, no defined peaks are observed beyond the first one at 2.7 Å, indicating the lack of clear solvent order beyond the first shell. The two pdf peaks in CHOH are located 2.8 and 5.5 Å away

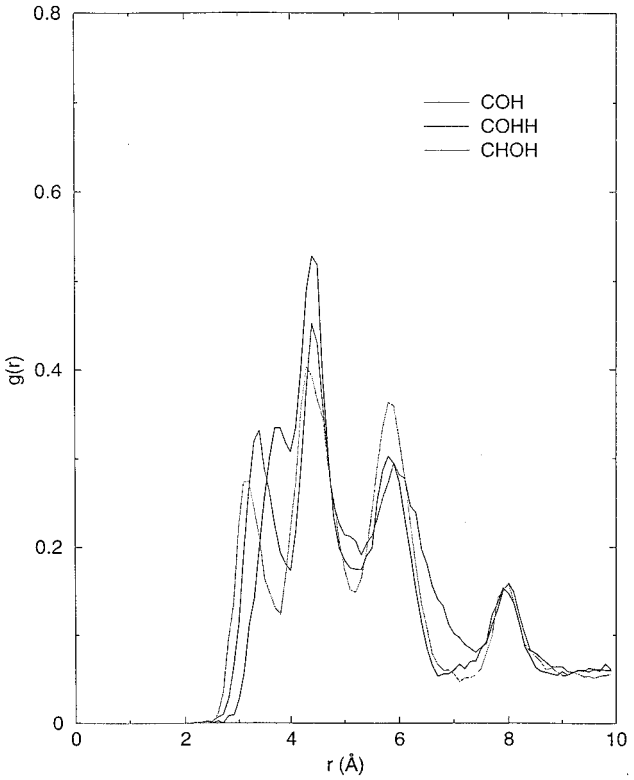

Figure 7. Pair distribution functions for the zinc ion to the oxygens in the surrounding water molecules.

from the oxygen of the zinc−water. The pdfs for oxygen in the zinc−hydroxide (COH and COHH) show nearly identical first peak intensity whereas the first peak for zinc−water (CHOH) is smaller. This stronger first solvent shell observed in COH and COHH is due to the more highly charged oxygen atom of the zinc−hydroxide ion than in the zinc-bound water case. The location of the first solvent shell also corresponds to experimental results where oxygen−oxygen pdfs for bulk water show a first peak at ∼2.8 Å.[44,45] Beyond the first peak, we observe deviations in the peak distances from the active site water. We have shown that the water ordering around the oxygen for the zinc−water/hydroxide is only similar in the first solvation shell for all three systems. Beyond that, different structuring for the water molecules in the active site cavity was observed, which is consistent with water bridge formation within the HCAII active site (see below).

The pdfs for the zinc ions show approximately four solvation shells around the ion for the three systems (Figure 7). There is a significant shift in the positioning of the first solvation shell (i.e., the first peak), while the remaining peaks are in good accord with one another. In the COH case the first peak (at ∼3.5 Å) is really a shoulder on a peak located at ∼4.5 Å. In COHH and CHOH, the first peak is distinctly separate from the second peak, and integration of the first peak shows only one water molecule is in this solvent shell. In CHOH, this peak is attributed to a water molecule that is occasionally found within 3 Å of the zinc ion but is not involved in water bridge formation (see below).

The pdfs for both ND1 and NE2 of His-64 to the oxygen of the water molecules show nearly identical solvent distributions for COH and CHOH. In the COHH system the ND1 and NE2 peak positions are similar to those seen for COH and CHOH, but with a higher peak intensity. There is, on average, an extra water molecule in the first solvation shell surrounding NE2@His-64 in COHH versus COH or CHOH. This is not surprising since His-64 in COHH is doubly protonated and, hence, positively charged. The second solvation shell is found ∼2 Å away from the first solvation shell. This distance is consistent with the formation of a water network radiating out from NE2 and ND1.

Table 4. Summary of Distance, Angle, and Percent Occurrence Data of the Glu-106−Thr-199−Zinc−Water/Hydroxide Hydrogen-Bonding Network

distance (Å)/angle (deg)	X-ray	COH	COHH	CHOH
OE1@Glu106−OG1@Thr199	2.6	2.6 ± 0.1	2.6 ± 0.1	2.6 ± 0.1
OG1@Thr199−O@Wat260	2.8	3.0 ± 0.2	3.0 ± 0.2	2.7 ± 0.1
OG1@199−H@260−O@260		141 ± 25	137 ± 27	157 ± 12
% H-bond occurrence		84.1	79.2	99.1

Experimentally, a "deep" water is found situated at the bottom of the active site and 3.4 Å away from the main chain N atom of Thr-199.[12] Thr-199 is positioned with Thr-200 on the opposite side of the active site cavity from the zinc atom. The deep water has been proposed to be involved in inhibitor and substrate binding.[12,36] In our simulations, we find the presence of a solvent shell ∼3 Å away from the nitrogen atom of Thr-199 in all three systems. The integration of this peak gives a value of about 1. This shows the presence of a long-lived "deep" water in the protein for all three stages of proton transfer.

Role of Glu-106 and Thr-199 in the Active Site. Thr-199, His-64, and Glu-106 combine with other polar residues to form the hydrophilic half of the active site cavity. The role of Thr-199 in the center between the hydrophilic and hydrophobic halves of the cavity has been the subject of many studies.[3,11,12] The hydrogen on the oxygen bonded to zinc is the hydrogen donor for a hydrogen bond to OG1 of Thr-199, and the hydrogen bound to OG1 (HOG) at Thr-199 is a hydrogen donor for a hydrogen bond to OE1 of Glu-106.[3,4,11] The proximity of Thr-199 to the active site zinc atom and the rigidity of this hydrogen bond network are considered to be crucial for catalysis and inhibitor binding.[14] This hydrogen bond network has been the subject of much speculation concerning its function.[3,12,15] It has been proposed that the role of this hydrogen bond network is to orient the nucleophilic zinc-bound hydroxide for optimal attack on the substrate.[11,14] A catalytic mechanism in which this network is involved in an intramolecular proton relay that interconverts the zinc−water and zinc−hydroxide has also been proposed by Kannan.[15] However, this would require the pK_a of Glu-106 to be unusually high (∼7.0 versus ∼4.0). Hence, this mechanism is generally discarded from consideration.[46]

Given the importance of this hydrogen bond network, we felt that it was important for us to analyze this particular active site feature. In all three simulations, we found that this hydrogen bond network is fairly well preserved. The average hydrogen bond distance in the COH system in the Zn−OH/H_2O···Thr-199···Glu-106 network is given in Table 4. Applying our hydrogen bond criteria (bond criteria, O−O < 3.5 Å; angular criteria, O−H−O > 120°; see below), we find that this hydrogen bond network in COH and COHH is present only 84.1% and 79.2% of the simulation time, respectively, whereas it is present for 99.1% of the time in CHOH. This shows that there is little or no disruption of the hydrogen-bonding network throughout the entire MD simulation for the zinc−water system (CHOH)

(44) Berendsen, H. J. C.; Grigera, J. R.; Straatsma, T. P. The Missing Term in Effective Pair Potentials. *J. Phys. Chem.* **1987**, *91*, 6289−6271.

(45) Soper, A. K.; Phillips, M. G. A New Determination of the Structure of Water at 25° C. *Chem. Phys.* **1986**, *107*, 47−60.

(46) Merz, K. M., Jr. Determination of pK_as of Ionizable Groups in Proteins: The pK_a of Glu 7 and 35 in Hen Egg White Lysozyme and Glu 106 in Human Carbonic Anhydrase II. *J. Am. Chem. Soc.* **1991**, *113*, 3572−3575.

but not for the zinc−hydroxide systems (COH and COHH). Analyzing the flexibility of the residues involved in this network, we observed a correlation between the RMSF of Glu-106 and Thr-199 (Table 2) and the ability to form the Glu-106···Thr-199···Zn−OH/H_2O hydrogen-bonding network. It appears that the higher conformational mobility of Glu-106 and Thr-199 in CHOH facilitates the high formation probability of this hydrogen-bonding network. The average angle between the hydroxyl oxygen of Thr-199, the hydrogen of zinc-bound water, and the oxygen of zinc-bound water (or hydroxide) is given in Table 4. While the angle for the two zinc−hydroxide cases (COH and COHH) shows similar values, the angle is significantly higher (by about 20°) for the zinc−water case (CHOH). This larger angle in the CHOH case may also facilitate the higher probability of Glu-106···Thr-199···Zn−H_2O network formation. Nonetheless, we have clearly shown that the role of this hydrogen bond network is to lock the Glu-106 and Thr-199 residues into their favorable geometries and that these residues show no inclination to vary from their positions.

Hydrogen Bonding and the Zinc to His-64 Water Bridge. Crystal structures have shown that the zinc ion in the active site is bound to three histidine groups and one water/hydroxide molecule tetrahedrally coordinated to the zinc ion.[3,4] Protonation of zinc−hydroxide does not change the tetrahedral arrangement around the zinc ion.[4] Many attempts have been made to explain the proton transfer in the active site of HCAII. It has been suggested that the zinc-bound water/hydroxide proton is not transferred directly to the external buffer, but through a rate-limiting proton-transfer group, His-64, on the enzyme, which facilitates the high catalytic activity of the enzyme.[10,21] A hydrogen bond network between the zinc-bound hydroxide and the imidazole side chain of His-64 through two intervening solvent molecules has been reported.[3,4] This network is important for catalysis where His-64 operates as a proton shuttle by accepting the proton (via the bridging solvent molecules) from the zinc-bound water. This leads to the regeneration of zinc-bound hydroxide, and subsequently the proton is passed along from His-64 to buffer. However, information obtained from the X-ray structure can only identify the water molecules that have low mobility and, hence, lack detailed dynamical information regarding the solvent structure in the HCAII active site. While the X-ray structures only identified two water molecules in the solvent bridge, theoretical gas-phase studies of HCAII using imidazoles to represent histidines by Lu and Voth concluded that the existence of a third water molecule in the water bridge is necessary for the proton-transfer channel to be efficient.[47] In a more recent classical MD simulation, Lu and Voth[48] have shown that the two-water-molecule bridge is the favored state in the zinc-bound water system as opposed to our observation of a four-water-molecule bridge (see below). Hence, the actual nature of the water bridge between the zinc ion and His-64 is a matter of controversy, and thus, the mechanism of proton transfer in HCAII is still relatively unexplained. This issue is explored further below.

In our simulations, we have evaluated the intraprotein interactions and solvent−solvent interactions through the presence or absence of hydrogen bond interactions. Similar studies on HCAII have been done by Lu and Voth.[48] However, in their simulations they used a cap of water for their system (i.e., the protein was not fully solvated) and very short simulations (∼100 ps), without the inclusion of long-range electrostatic interactions using the Ewald sum methodology. Their long-range electrostatic interactions were modeled after the extended model by Stote et al.[49] In addition, only the zinc-bound water (corresponding to our CHOH system) state was reported in their paper.[48] Our MD simulations have addressed these limitations, and we feel that our study provides a more detailed and accurate representation of the intramolecular proton transfer in HCAII. The criteria used for a hydrogen bond in this research were solely geometric. For the solvent−solvent hydrogen bond calculation, we consider a solvent hydrogen bond to be present if both distance (e.g., O−O < 3.5 Å) and angular (e.g., O−H−O > 120°) criteria are satisfied simultaneously. The starting crystal structure used in our simulations showed that the ND1 of His-64 is connected with the zinc-bound water through two water molecules with oxygen−oxygen distances of 2.7 and 3.2 Å.[4] However, the crystal structure lacks hydrogen atom information to allow insight into the particular types of hydrogen bonding. Hydrogen bonding in water networks can be categorized using three different models:[50] sequential hydrogen bonding, which was found to be the most energetically favored, the alternative double donor hydrogen binding, and the double acceptor hydrogen bonding. The different energetic states are clearly observed in our three systems. For example, the preferred state in the COH system is when the zinc−hydroxide forms a hydrogen bond to the hydrogen of a water molecule, and the same water molecule donates its other hydrogen (hence, double donor) to the second water molecule in the network (see Figure 8). In all three systems, the bridging water molecules were observed to undergo rotational motion, thereby exchanging the hydrogen bond from proton H1 to proton H2 (and vice versa) for the same donor and acceptor atoms. The ability of water molecules to undergo rotation without disrupting the hydrogen-bonding network not only shows the dynamic nature of the water molecules, but also shows the stability of the solvent network once it is formed (i.e., the energetically favored water network, once formed, is not easily disrupted).

The water bridge network formed in COH ranges from three to five water molecules, with the three-water-molecule network being the most common one (Figure 9). This water bridge has calculated lifetimes ranging from 1 to 15 ps. We define each water bridge as containing several distinct water molecules. When another water molecule diffuses in and replaces an existing water molecule in the water bridge, we consider that to be a new water bridge. In COH, we observed about 15 different water bridges. Hence, while each water bridge formed has a short lifetime, we occasionally observe several water bridges continuously contributing to a water bridge network lasting ∼100 ps. This is consistent with the experimentally determined rate constants for proton-transfer reactions between imidazolium and water, which are on the order of 10^{10} M^{-1} s^{-1}.[51] The probability of water bridge formation can also give us a qualitative insight into the free energy barrier resulting from the formation of a water bridge. The total (i.e., all water bridge lengths were considered) probability of water bridge formation is defined as the number of frames with a water bridge versus the total frames of the analyzed trajectory. In COH, the probability of water bridge formation is 39%. The free energy

(47) Lu, D.; Voth, G. Proton Transfer in the Enzyme Carbonic Anhydrase: An ab initio Study. *J. Am. Chem. Soc.* **1998**, *120*, 4006−4014.

(48) Lu, D.; Voth, G. A. Molecular Dynamics Simulations of Human Carbonic Anhydrase II: Insight Into Experimental Results and the Role of Solvation. *Proteins: Struct., Funct., and Genet.* **1998**, *33*, 119−134.

(49) Stote, R. H.; States, D. J.; Karplus, M. On the Treatment of Electrostatic Interactions in Biomolecular Simulation. *J. Chem. Phys.* **1991**, *88*, 2419−2433.

(50) Jeffrey, G. A.; Saenger, W. *Hydrogen Bonding in Biological Structures*; Springer-Verlag: Berlin, Germany, 1991.

(51) Sudmeir, J. L.; Evelhoch, J. L.; Jonsson, B.-H. Dependence of NMR Line shape Analysis upon Chemical Rates and Mechanisms: Implications for Enzyme Histidine Titrations. *J. Magn. Reson.* **1980**, *40*, 377−390.

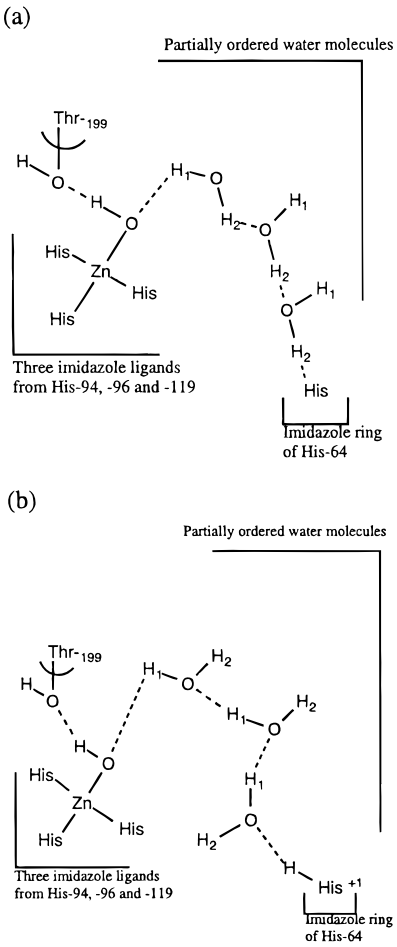

Figure 8. Schematic drawing for the intramolecular proton transfer from zinc−hydroxide to His-64 in the active site of HCAII via (a) a double donor hydrogen-bonding network and (b) a sequential hydrogen-bonding network which is energetically favored. In addition to water diffusion, the water molecules can undergo rotational motion, and hence, the hydrogens (labeled H_1 and H_2) involved in the solvent network may vary at different times.

of water bridge formation (ΔF) can then be directly calculated from the probability of bridge formation. This is expressed as

$$\Delta F = -RT \ln P$$

where R is the gas constant, T is the temperature, and P is the probability. This correlation allows us to estimate the energy barrier height due to solvent reorganization, which when combined with the intrinsic barrier height (variously estimated to be 8−10 kcal/mol[47,52]) gives the total proton-transfer barrier. An experimental estimate of the intrinsic and overall energy barrier involved in the intramolecular proton transfer in human carbonic anhydrase III by Silverman et al. showed the need to consider the energetic contributions arising from solvent/protein reorganizations.[52] Using the correlation above, the calculated free energy of water bridge formation for COH is ∼0.56 kcal/mol. In COHH, the solvent bridge observed involves two to three bridging water molecules, with two water molecules being the most common. No solvent channels involving more than three mediating water molecules to His-64 were observed in COHH. The solvent channels observed in COHH occurs only through sequential hydrogen bonding. Applying the same

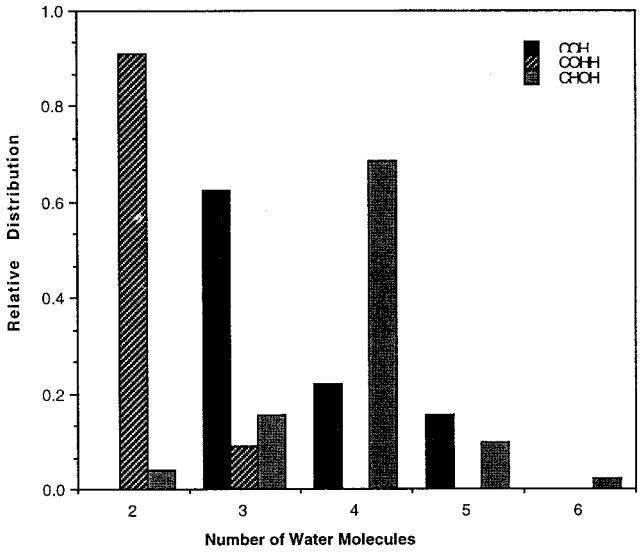

Figure 9. Relative distribution of the number of water molecules participating in the solvent bridge network between zinc−water/hydroxide and His-64. The COHH system favors the shortest water bridge followed by COH and CHOH.

hydrogen-bonding criteria, we observe that the probability of solvent bridge formation is ∼16%, which corresponds to a free energy of formation of 1.11 kcal/mol. The average lifetime of the solvent bridge in COHH varies from 3 to 15 ps, and only four different water bridges were observed. In CHOH, we observed a total of nine different water bridges with two to six water molecules participating in the solvent network (Figure 9) with a free energy of formation of 1.57 kcal/mol and an average lifetime of ∼1 ps. Although the preferred number of water molecules for the solvent bridge formation in CHOH is four (Figure 9), the distribution of water molecules participating in solvent bridge formation is greater than in COH or COHH. This preference for the longer solvent bridge in CHOH is very interesting. In a study of intramolecular proton transfer in the gas phase, Liang and Lipscomb found that the proton transfer along longer water chains is favored due to smaller repulsions between the positive zinc ion and the proton in a longer water chain.[53] This is in contrast to the findings of Lu and Voth in which two water molecules were involved in the favored water bridge length.[48] Our simulations corroborate the Liang and Lipscomb[53] findings, with the zinc ion in COHH having the smallest positive charge and favoring the least number of water molecules in the solvent bridge, and the zinc ion in CHOH having the highest positive charge and favoring the longer water chains for solvent bridge formation. At the same time, the higher number of participating water molecules also makes the water bridge in CHOH more susceptible to solvent reorientation and exchange due to the longer length of the water chain and, hence, the shorter water bridge lifetime.

The free energy of water bridge formation is largest for CHOH followed by COHH and COH. Although the free energy results are not quantitative, the trend is obvious for the favored stage in the intramolecular proton process. Our qualitative results are consistent with experimental and theoretical results,[47,54] where the initial proton transfer from the zinc-bound water to

(52) Silverman, D. N.; Tu, C.; Chen, X.; Tanhauser, S. M.; Kresge, A. J.; Laipis, P. J. Rate-Equlibria Relationships in Intramolecular Proton Transfer in Human Carbonic Anhydrase III. *Biochemistry* **1993**, *32*, 10757−10762.

(53) Liang, J.-Y.; Lipscomb, W. N. Hydration of CO_2 by Carbonic Anhydrase: Intramolecular Proton Transfer between Zn^{2+}-Bound H_2O and Histidine 64 in Human Carbonic Anhydrase II. *Biochemistry* **1988**, *27*, 8676−8682.

(54) Taoka, S.; Tu, C.; Kistler, K.; Silverman, D. N. Compariosn of Intra- and Intermolecular Proton Transfer in Human Carbonic Anhydrase II. *J. Biol. Chem.* **1994**, *269*, 17988−17992.

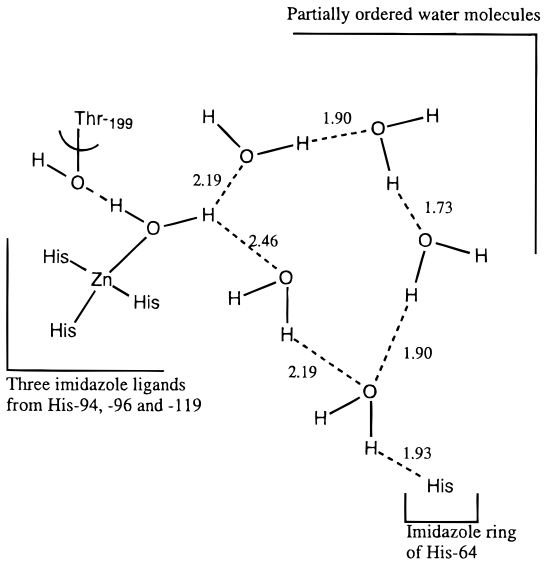

Figure 10. Schematic drawing for the 510 ps snapshot of the CHOH system. Note the coexistence of two possible water bridges from zinc-bound water to His-64. The numbers associated with the dashed lines give the hydrogen-bonding distance. Although the four-water-molecule-containing bridge is preferred in CHOH, it can easily collapse to a two-water-molecule bridge favored in the COHH system due to the positioning of the water molecules in the network.

the first bridging water to form a zinc-bound hydroxide and hydronium ion is rate limiting, with subsequent proton transfers between hydronium ions and adjacent water molecules having much smaller barrier heights. On the basis of the study of HCAII by Lindskog, the thermodynamic free energy difference between the two stages of the intramolecular proton transfer (corresponding to CHOH and COHH) is −0.37 kcal/mol.[55] We find that the difference in the free energy of water bridge formation in the CHOH and COHH in our simulation is −0.46 kcal/mol. If we consider the water bridge formation as the primary driving force for the transition between CHOH and COHH, our estimated free energy values correspond closely to the experimental value. Although the free energy of water formation values obtained are applicable to each particular state, and we are not able to obtain the activation energy (i.e., barrier height) between the two stages, our energetic difference results indicate that intramolecular proton transfer from zinc-bound water to His-64 through a solvent bridge is feasible. Our results further provide theoretical support for the proton-transfer mechanism via His-64 in HCAII.

We note that although we have excluded the solvent bridge containing two water molecules in the COH system for not meeting the cutoff criteria used in this study (either angle or distance cutoff), the two-water-molecule bridge does occasionally coexist with the three-water-molecule bridges. Similarly, we have observed the same coexistence of a solvent bridge containing different numbers of water molecules in CHOH (Figure 10). Nevertheless, it has been shown that the number of water molecules involved in the proton relay does not seem to affect the intrinsic reaction barrier for intramolecular proton transfer.[53] In the X-ray structure, alternate solvent channels were also observed where water molecule 292 is part of a two-water solvent bridge with water 318 between zinc-bound hydroxide and His-64 in the native enzyme, and water molecules 264 and 369 are part of alternate, three-water solvent bridges between water 292 and His-64 (i.e., zinc−hydroxide···water 318···water 292···water 264/369···His-64). Since only high-occupancy water molecules can be observed in the X-ray structure, it is possible that the more dynamic water molecules that may have formed other alternate water bridges with more water molecules were not observed.

Plots of the oxygen atoms of the water molecules participating in the solvent bridge network as a function of distance from the zinc ion and CA@His64 are given in Figure 11. These plots give us a spatial insight into the positions of the water molecules in the active site that are involved in the water bridge network. The four water molecules from the X-ray structure (water 318, 292, 264, 369) that are part of the two-water solvent bridge network, or the alternate three-water solvent bridge, are shown as triangles. The water molecules from the simulations that are part of the most favored solvent network are marked with x's: In other words, only water molecules involved in the two-water solvent bridge in COHH, three-water solvent bridge in COH, and four-water solvent bridge in CHOH are included. While both the COHH and COH systems show similar scatter of the water positions, the water bridge network in COHH corresponds more closely to the two-water solvent bridge (water 318 and 292) in the X-ray structure. This similarity of water bridge between the COHH system and the X-ray structure suggests the possibility that His-64 in the X-ray structure may have been doubly protonated rather than singly protonated. This is not surprising given that the crystal structure was refined at pH 7.8, which is close to the His-64 pK_a of 7.1, and hence, His-64 in the crystal structure may have been doubly protonated. In addition, hydrogen atoms are not experimentally observable in X-ray structures, so the assumption that His-64 remained singly protonated in the pH 7.8 crystal structure is a matter of debate. In the CHOH system, there is more scatter in the positions of the solvent bridge water molecules, and only a weak correlation between the positions of water molecules from the X-ray structure and the simulation was observed. This suggests that the water bridge in the CHOH system is unstable. This result is consistent with X-ray studies of HCAII with zinc-bound water (determined at pH 5.7) by Nair et al., where the solvent bridge between His-64 and the zinc-bound water was absent.

Our simulations have further shed some light on the dynamic nature of the water bridge formation. We have observed the existence and coexistence of several water bridges where two to six water molecules may participate in the water bridge formation between the zinc−water/hydroxide and His-64. These partially ordered water molecules forming the water bridge are both indirectly and directly important for the intramolecular proton transfer. In addition, we observe that the water molecules in the solvent bridge, while remaining ordered, undergo constant rotational motion. This shows that water molecules in the proton-transfer relay are not trapped in a single conformation but rather have full rotational freedom. The next question is whether the proton transfer occurs via concerted or sequential motion. The study by Scheiner et al. of multiple proton transfers showed that the sequential and concerted proton transfers yield the same energy barriers.[56] The variations in rotational motions observed for the water molecules in the solvent bridges in our simulations support the notion that multiple barriers may exist within the solvent bridge network, and hence, the sequential proton-transfer mechanism would be favored. Clearly, this is a qualitative conclusion, and more studies need to be done in this area.

We have also calculated the intraprotein hydrogen bonds to obtain insights into the stability of the protein at the different stages in proton transfer. For this purpose, all polar hydrogens

(55) Lindskog, S. The Kinetic Mechanisms of Human Carbonic Anhydrases I and II: A Computer Approach. *J. Mol. Catal.* **1984**, *23*, 357−368.

(56) Scheiner, S. *J. Am. Chem. Soc.* **1981**, *103*, 315.

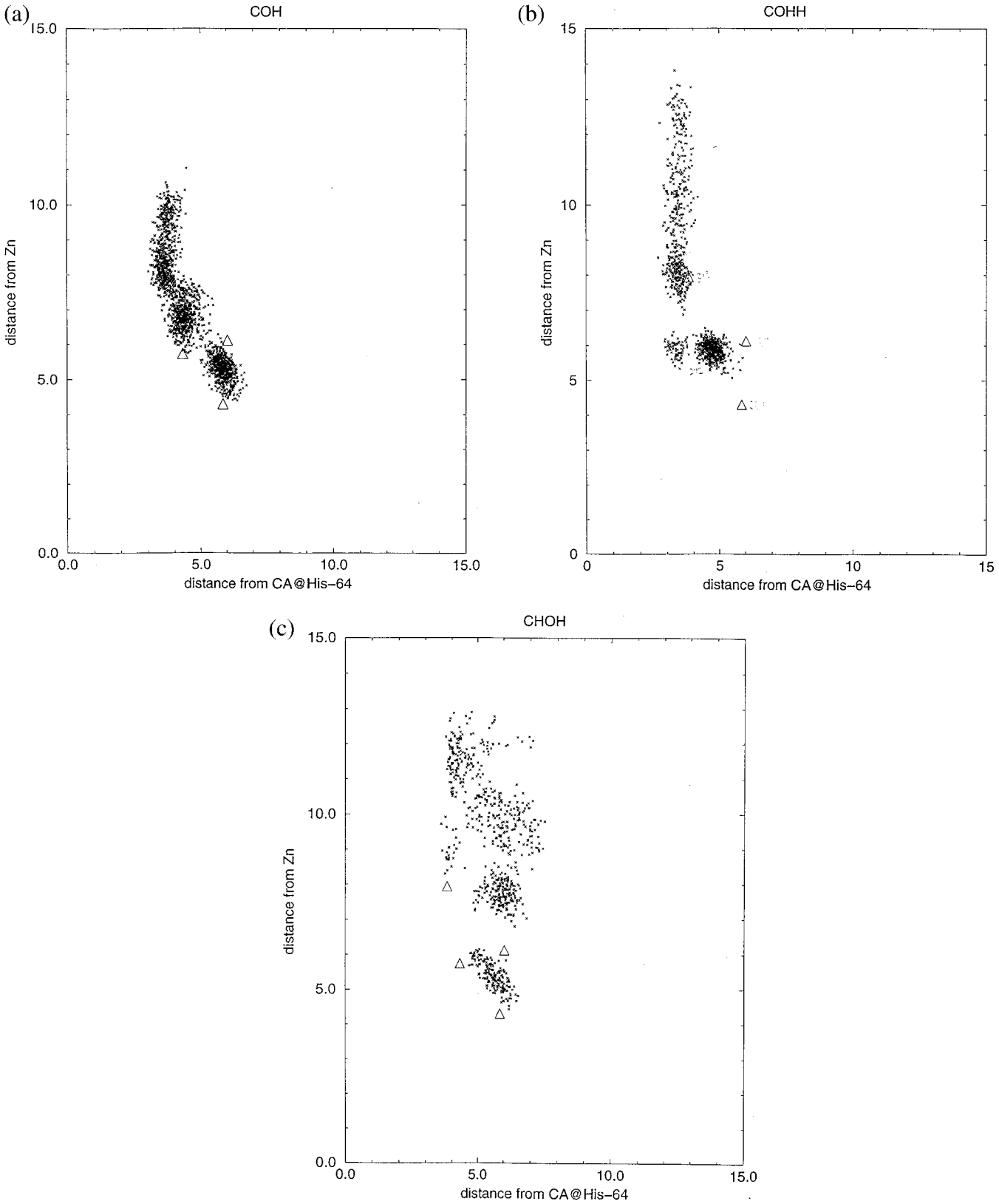

Figure 11. Scatter plot of the solvent distribution of water molecules in the active site that participate in the most favored water bridges. The oxygens of the water molecules are marked as x, and the triangles mark the water molecules from the X-ray structure. The positions are plotted as a function of the distance of the oxygen of the water molecules from zinc ion and CA@His64. (a) COH, (b) COHH, and (c) CHOH.

were identified and distances to potential hydrogen bond acceptors were calculated. If the hydrogen atom−acceptor atom distance was less than 2.6 Å and the angle between the hydrogen bond donor atom, hydrogen atom, and acceptor atom was between 120° and 180°, then a hydrogen bond was considered to exist.[57] We were also interested in the stability of the hydrogen bond. A hydrogen bond is considered to be stable if it exists for ≥90% of the trajectory time. In our simulations, variations in the total number of hydrogen bonds that were formed throughout the trajectories were observed for the three

Table 5. Average Values of Backbone and Side Chain Dihedral Angles for His-64

His-64	χ_1 (deg)	χ_2 (deg)	ψ (deg)	φ (deg)
X-ray[a]	−16.5	−68.8	−13.8	−121.6
X-ray[b]	43.9	95.0	−18.7	−127.3
COH	65 ± 10	86 ± 12	−24 ± 9	−131 ± 11
COHH	61 ± 7	90 ± 9	−27 ± 9	−129 ± 11
CHOH	58 ± 11	95 ± 14	−25 ± 10	−131 ± 11

[a] X-ray structure from Nair et. al. with the His-64 side chain in the "out" position. [b] X-ray structure from Håkansson et al. with the His-64 side chain in the "in" position.

systems (see Table 2). However, it is interesting to note that if we only consider the stable hydrogen bonds (≥90%) as the predominant contributors to protein stability, there is almost no difference in the number of hydrogen bonds in the three different systems. This is indicative of the stability of the protein during all three stages of the intramolecular proton-transfer reaction.

Role of His-64 in the Proton-Transfer Mechanism. The position of His-64 is of particular interest because it is generally accepted that it is an important basic site in rate-limiting proton relays.[1] His-64 has been reported to exist in two conformations.[58,59] The orientation of His-64 (i.e., ring flipping) has been observed to depend on pH.[59] At high pH, the imidazole side chain of His-64 is directed toward the active site and is designated as the "in" conformation. Conversely, the His-64 side chain is in the "out" conformation at low pH and closer to the more hydrophobic region defined by Trp-5, Gly-6, Tyr-7, and Phe-231.[3] Hence, the conformation of His-64 is generally regarded as being sensitive to the changes in solvent structure which, in turn, arise from changes in protein structure, counterion concentration, or pH.[27] Nevertheless, the different conformations for His-64 will not hinder efficient proton transfer in catalysis as long as the solvent structure can satisfactorily accommodate the different conformations.[59]

To obtain insights into the conformational mobility (i.e., ring flipping) of His-64, we have calculated the torsional values χ_1 (N−CA−CB−CG) and χ_2 (CA−CB−CG−ND1). The study by Nair and Christianson[59] showed that, at lower pH, the side chain of His-64 rotates away from the active site by 64° around χ_1. The average values of χ_1 and χ_2 from our simulations are given in Table 5. Although there is a lot of scatter in the plot, which indicates some conformational mobility of the side chain, the average values of χ_1 and χ_2 for the three systems are located within the same region, indicating the same favored conformation. Hence, despite its presumed mobility, the side chain of His-64 has remained in the "in" conformation in all three stages of proton transfer. Our results further support the experimental data where the "in" conformation of the His-64 side chain is preferred for proton transfer and in the absence of inhibitor binding in HCAII.[3,4,12] For example, His-64 of HCAII rotates to the "out" conformation in order to accommodate the binding of thienothiopyran-2-sulfonamides in the enzyme active site.[60]

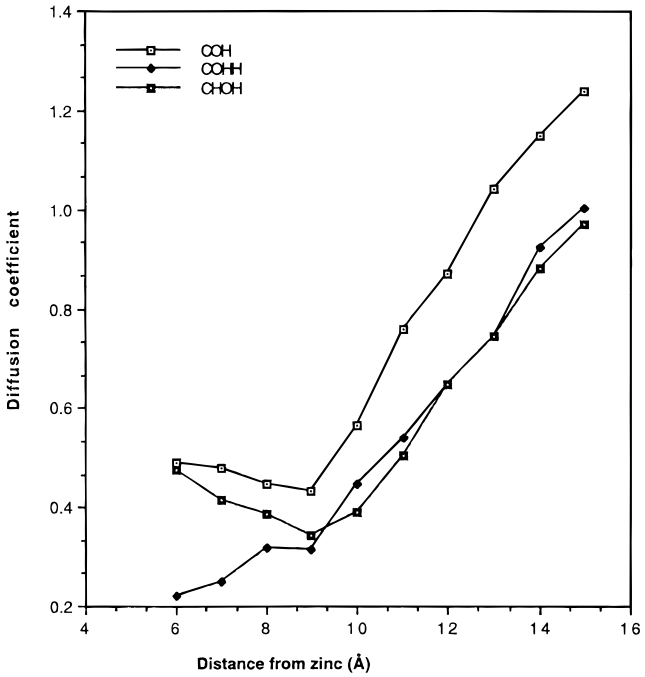

Figure 12. Calculated diffusion coefficients for solvent molecules as a function of the zinc ion distance. Distances of less than 9 Å indicate the diffusion coefficients for solvent molecules within the active site cavity.

Although the conformational mobility of His-64 has been proposed as a factor that is important in the catalytic mechanism[27,42,58] (especially for the intermolecular proton-transfer process), it has also been suggested that the intramolecular proton transfer does not depend on a specific orientation of the imidazole ring as proton acceptor.[54,58] If we assume that the force field representation of the conformational preferences for His-64 is realistic, then our observation that His-64 remains in the "in" orientation suggests that (1) the time scale for ring "flipping" is longer than our simulated time scales, (2) the ring flip is sensitive to other changes occurring in the vicinity of His-64 (e.g., change in a protonation state, local conformational changes, etc.) which we have not modeled, or (3) the ring flip is not critical for the intramolecular and possibly the intermolecular proton transfer. At this point, the issue of how critical the flexibility of His-64 (or the lack of) is for efficient proton transfer is still open for debate.[61]

We have also calculated the ψ and the φ torsional values to obtain an insight into the backbone conformations of His-64, and the average torsional values are given in Table 5. In all three systems, His-64 retains the same backbone conformation, which is close to the values obtained from the X-ray structure.[4] The ability of His-64 to retain its backbone conformation, as part of the secondary structure, is essential in maintaining its position in the protein. The strategic positioning of His-64 at the interface between bulk solvent and solvent within the active site is important for the role of His-64 as an efficient proton shuttle group.[3,4,61] The role of His-64 as the gate-keeper of the solvent interface is further evidenced from our diffusion coefficient calculation as a function of distance from the zinc ion (see Figure 12). The diffusion coefficient plot as a function of distance from the zinc ion given in Figure 12 shows two distinct solvent regions with different mobilities. The water molecules within the active site have a low diffusion coefficient,

(57) Tirado-Rives, J.; Jorgensen, W. L. Molecular Dynamics of Protein with the OPLS Potential Functions. Simulation of the Third Domain of Silver Pheasant Ovomucoid in Water. *J. Am. Chem. Soc.* **1990**, *112*, 2773−2781.

(58) Krebs, J. F.; Fierke, C. A.; Alexander, R. S.; Christianson, D. C. Conformational Mobility of His-64 in the Thr → Ser Mutant of Human Carbonic Anhydrase II. *Biochemistry* **1991**, *30*, 9153−9160.

(59) Nair, S. K.; Christianson, D. W. Unexpected pH-Dependent Conformation of His-64, the Proton Shuttle of Carbonic Anhydrase II. *J. Am. Chem. Soc.* **1991**, *113*, 9455−9458.

(60) Baldwin, J. J.; Ponticello, G. S.; Anderson, P. S.; Christy, M. E.; Murcko, M. A.; Randall, W. C.; Schwam, H.; Sugrue, M. F.; Springer, J. P.; Gautheron, P.; Grove, J.; Mallorga, P.; Viader, M.-P.; McKeever, B. M.; Navia, M. A. *J. Med. Chem.* **1989**, *32*, 2510−2513.

(61) Jackman, J. E.; Merz, K. M., Jr.; Fierke, C. A. Disruption of the Active Site Solvent Network in Carbonic Anhydrase II Decreases the Efficiency of Proton Transfer. *Biochemistry* **1996**, *35*, 16421.

but beyond 9 Å from the zinc ion (which is roughly the position of His-64; see Table 3), the diffusion coefficient values increase rapidly toward the bulk solvent values. The low solvent mobility within the active site is important in maintaining the water bridge network for intramolecular proton-transfer relay. Simultaneously, the high solvent mobility of the bulk solvent allows fast intermolecular proton transfer to occur. The side chain of His-64 is solvent exposed at the beginning of our simulations and remains solvent exposed throughout the simulations.

Conclusions

This study has been primarily aimed at investigating the role of water molecules in the active site of HCAII in the intramolecular proton-transfer relay. We have approached this question using MD simulations of the systems representing the three different stages of the proton-transfer process. Using an electrostatic representation derived from QM/MM calculations, in conjunction with a bonded model[26] for the zinc ion, we have been able to accurately reproduce the tetrahedral geometry coordination of the zinc ion in the HCAII active site. Our approach has proved to be a viable method for obtaining insights into the protein and solvent dynamics at the intermediate stages in the proton-transfer relay. From the results presented in the previous sections, some conclusions can be drawn.

It has been proposed that the presence of a water bridge is necessary for the intramolecular proton transfer from zinc-bound water to His-64.[1,3,10,16,17,48] Our analysis shows that the number of water molecules forming the water bridge in the active site can vary from two to six. This particular insight into the active site water dynamics has not been observed previously in X-ray structures.[3,4] X-ray structures only indicate two, high-occupancy, water molecules in the solvent bridge and may not have been able to observe other solvent bridges which are relatively short-lived. Other studies have also shown that a longer water bridge (greater than two water molecules) is favored[53] and necessary for efficient proton transfer.[47] Occasionally, the coexistance of several water bridges has been observed in our simulations. These simulations have given us insights into the different hydrogen-bonding arrangements possible in the water bridge; sequential hydrogen bonding is preferred in COHH and CHOH while the double donor orientation is the favored hydrogen-bonding pattern in COH. We also find that the water molecules undergo rotational motion while in the solvent bridge. The free energy of water bridge formation is found to be highest in CHOH, followed by COHH and COH.

We find that the active site cavity in HCAII allows the protein to experience two distinctly different solvent environments. These two solvent regions can be defined as the region containing solvent molecules within the active site and the region containing solvent molecules located outside the active site (i.e., bulk solvent). The low solvent mobility for the water molecules within the active site is crucial for maintaining the proton-transfer relay present between the zinc−water/hydroxide and His-64. His-64, located at the mouth of the active site cavity, is the gate-keeper that separates the two solvent regions. The side chain of His-64 remained in the "in" (facing the active site) position in all cases, and doubly protonated His-64 had significantly more conformational flexibility than neutral His-64. It has been proposed that the two experimentally observed conformations for His-64 do not hinder proton transfer as long as the solvent structure can satisfactorily accommodate them.[59] However, on the basis of our results, we feel that there is a correlation between His-64 and the solvent molecules. Contrary to the mainly rigid residues in the active site cavity, the higher flexibility of the His-64 side chain allows it to find the optimum geometry between the active site solvent molecules and the bulk solvent. This is clearly more evident in COHH where the high flexibility of His-64 is crucial for its imidazolium side chain to be an efficient proton-transfer agent.

While the residues surrounding the active site cavity remained rigid for all three systems, the surface residues, near the mouth of the active site cavity, in the COHH system showed unusually high flexibility. We propose that the role of the surface residues (with their high flexibilities) is to perturb the solvent molecules around the surface of the protein and near the active site cavity entrance. Hence, this allows for water and buffer exchange surrounding His-64 and helps facilitate intermolecular proton transfer. The flexibility of His-64 and the surface residues possibly contributes to the fast kinetics observed in HCAII proton transfer to bulk solvent or buffers.

In addition, these simulations have given us insights into the dynamics of the hydrophobic packing within the protein's interior. The hydrophobic core of the protein, being adjacent to His-64, is perturbed by the charged environment of the doubly protonated state of His-64. The protonation of the His-64 side chain in COHH resulted in greater fluctuations of residues in the lower hydrophobic core. Finally, we observe that the hydrogen-bonding network between Glu-106, Thr-199, and Zn−water/hydroxide is longer-lived in CHOH. This may be due to the higher flexibility of the Glu-106 and Thr-199 side chains which can better accommodate the structural fluctuations found in the bonds and angles. This stable hydrogen-bonding network, in turn, helps to lock the zinc−water in the favored orientation for the transfer of a proton to the neighboring water molecule in the proton-transfer relay.

Acknowledgment. We thank the NIH for supporting this research through Grant GM44974. We also thank the Pittsburgh Supercomputer Center, National Center for Supercomputer Applications, San Diego Supercomputer Center, and Cornell Theory Center for generous allocations of supercomputer time.

JA983579Y